Bacterial transport of colloids in liquid crystalline environments: Supplementary Material

Rishi R. Trivedi,[1] Rina Maeda,[1] Nicholas L. Abbott,[2] Saverio E. Spagnolie,[3] and Douglas B. Weibel[1,4,5]

[1]*Department of Biochemistry, University of Wisconsin-Madison, 440 Henry Mall, Madison, WI 53706, USA.*
[2]*Department of Chemical and Biological Engineering, University of Wisconsin-Madison, 1415 Engineering Dr., Madison, WI 53706, USA.*
[3]*Department of Mathematics, University of Wisconsin-Madison, 480 Lincoln Dr., Madison, WI 53706, USA.*
[4]*Department of Chemistry, University of Wisconsin-Madison, 1101 University Ave., Madison, WI 53706, USA.*
[5]*Department of Biomedical Engineering, University of Wisconsin-Madison, 1550 Engineering Dr., Madison, WI 53706, USA.*

SUPPLEMENTARY MOVIE CAPTIONS

Movie S1. Bright field optical microscopy video showing *P. mirabilis* cells in 15 wt% DSCG at 25^{circ}C (nematic phase) carrying yeast cells along the far field LC director ($\boldsymbol{n}$), aligned in the x-direction (horizontal direction of movie).

Movie S2. Bright field optical microscopy video depicting multiple *P. mirabilis* cells pushing a group of yeast (*Candida albicans*) along a curved path following the director profile.

Movie S3. Bright field optical microscopy video demonstrating that *P. mirabilis* cells pushing 2-μm microparticle along the LC director ($\boldsymbol{n}$).

EXPERIMENTAL SETUP

Bacterial and yeast strains and cell culture

P. mirabilis strain HI4320 over-expressing the pflhDC plasmid was used in this study. HI4320 is a clinical strain isolated from a patient with urinary catheter-associated bacterial infection. The pflhDC plasmid contains the flhDC genes encoding the expression of FlhD and FlhC, and was inserted into pACYC184. pflhDC plasmid was transformed into wild- type strain HI4320 by electroporation and transformants were selected on lysogeny broth (LB) (1% [w/v] tryptone, 0.5% [w/v] yeast extract, and 1% [w/v] NaCl) agar plates (3% [wt/vol]) containing chloramphenicol (34 μg mL^{-1}). Overnight culture of *P. mirabilis*-flhDC cells were grown in nutrient rich medium consisting of 1% (wt/vol) peptone (Becton, Dickinson, Sparks, MD), 0.5% (wt/vol) yeast extract (Becton, Dickinson), and 1% (wt/vol) NaCl (Fisher Scientific, Fairlawn, NJ) with 34 μg mL^{-1} of chloramphenicol for 12-16 h at 30 °C with agitation (200 rpm). Saturated overnight culture was diluted (1:100) in fresh growth media containing 34 μg mL^{-1} of chloramphenicol, incubated at 30 °C with agitation (200 rpm) for 4 h until the absorbance (λ=600 nm) reached 3.0 to harvest cells at their peak motility. Colonies of *Candida albicans* cells were grown LB agar plates, picked directly, and suspended in liquid for experiments.

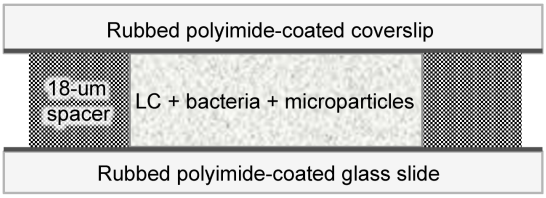

Figure S1. A schematic representation of the experimental chamber used to observe the motility of bacterial cells in LC solutions. The double-headed arrows indicate the direction of rubbing along the surface of the glass slides.

Lyotropic LC preparation

Disodium cromoglycate (DSCG) was purchased from Sigma-Aldrich (Milwaukee, WI) and used as received. Lyotropic LCs containing DSCG were prepared by mixing 15.3 wt% of DSCG with 84.7 wt% of aqueous motility buffer. The mixture was shaken for at least 12 h to ensure complete solubility and homogeneity. Prior to experimentation, the DSCG solution was heated at 65°C for 10 min to avoid possible time dependence of the properties of the mixture by melting the LC solution homogeneously. After cooling the solution to 25°C, a small volume of motility buffer containing bacteria and microparticles was added to the DSCG mixture to get final 15.0 wt% DSCG concentration for all experiments.

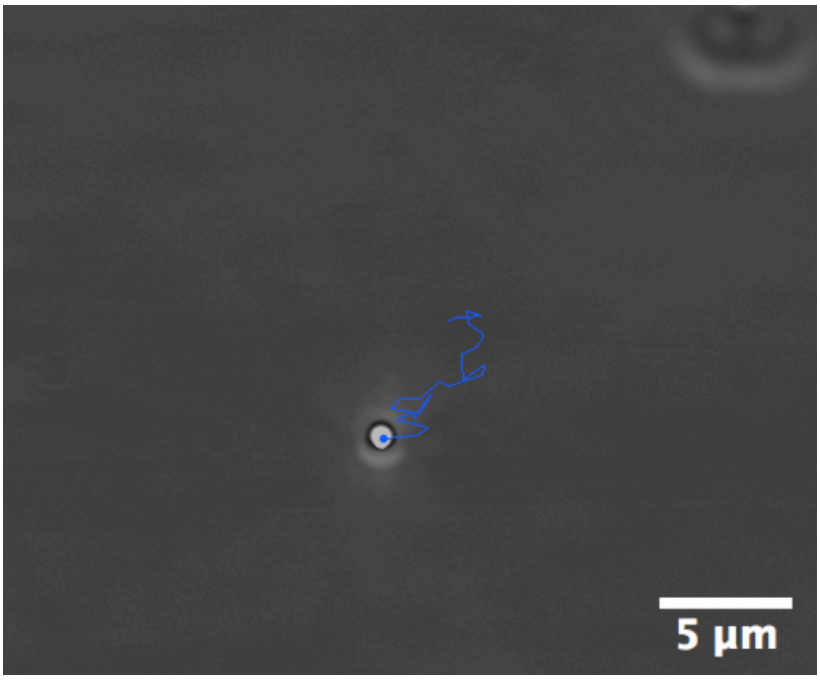

Figure S2. Phase contrast microscope image of a 1-μm diameter polystyrene microparticle diffusing in nematic DSCG at 25 °C. The blue line in the image indicates the superimposed trajectory of the drifting microbead recorded every 1 min over 30 min.

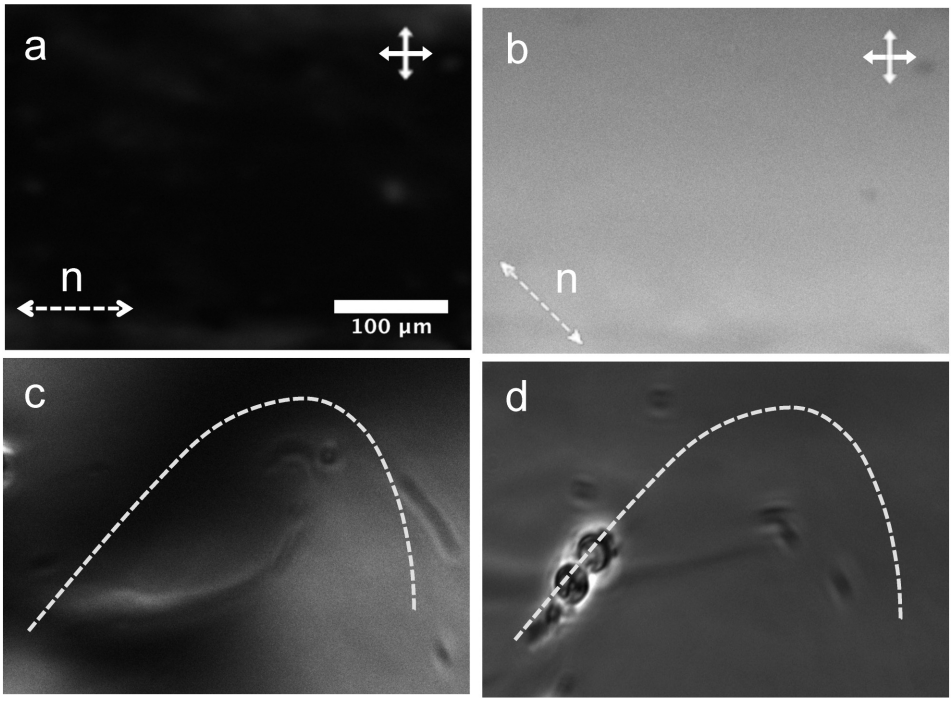

Figure S3. Polarized light micrographs of the experimental chamber aligned (a) parallel and (b) 45° to one of the crossed polarizers. We confirmed that the alignment of the nematic LC was parallel to the direction of rubbing by inserting a quarter wave plate into the optical path of a microscope and analyzing the appearance of the sample between crossed polars. (c) and (d) represent the local alignment of the LCs under crossed polars and bright field respectively. Dotted line represents the complex director profile by using bacteria as a tracer of local director.

Materials

DSCG (>95%) was from Sigma. Polystyrene microparticles with diameters of 1, 1.75 (fluorescent), 2, and 3 μm were from Polysciences. We rinsed microparticles with motility buffer [0.01 M KPO_4, 0.067 M NaCl, 10^{-4} M EDTA (pH 7.0)] before performing experiments.

Measuring the velocity of cells pushing microparticles

We measured the velocity of individual *P. mirabilis* cells (in μm s^{-1}) using the ImageJ manual tracking plugin[1]. A 1 mL aliquot of a suspension of cultured cells (absorbance of 3.0-3.5, λ = 600 nm) was concentrated by centrifugation for 5 min at 1000 rpm at 25 °C, and the cell pellet was gently resuspended in 50 μL of motility buffer containing 0.1 M glucose and 0.001% (w/v) Brij-35. 40μL stock solution of microparticles were washed twice in the motility buffer and resuspended in 200μL of motility buffer. Microparticles and cell suspension were added in 1:1 ratio in 15.3 wt% DSCG stock solution. After gently mixing LC, microparticles and bacteria, 1 μL of the solution was spotted on a pre-cleaned slide glass with two spacers (18-μm thick). The experimental chamber was covered with a 1.5 mm glass coverslip and sealed with Epoxy. We imaged cell motility using a Nikon Eclipse Ti equipped with a Photometrics CoolSNAP HQ2 CCD camera (Photometrics, Tucson, AZ). Images were acquired using a ×100 (Nikon Plan APO) oil immersion objective and the NIS-Elements AR microscope imaging software program (Version 4.000.07) (Nikon, Melville, NY). Videos were collected at 11.05 frames per second with 100ms exposure time and EM gain off.

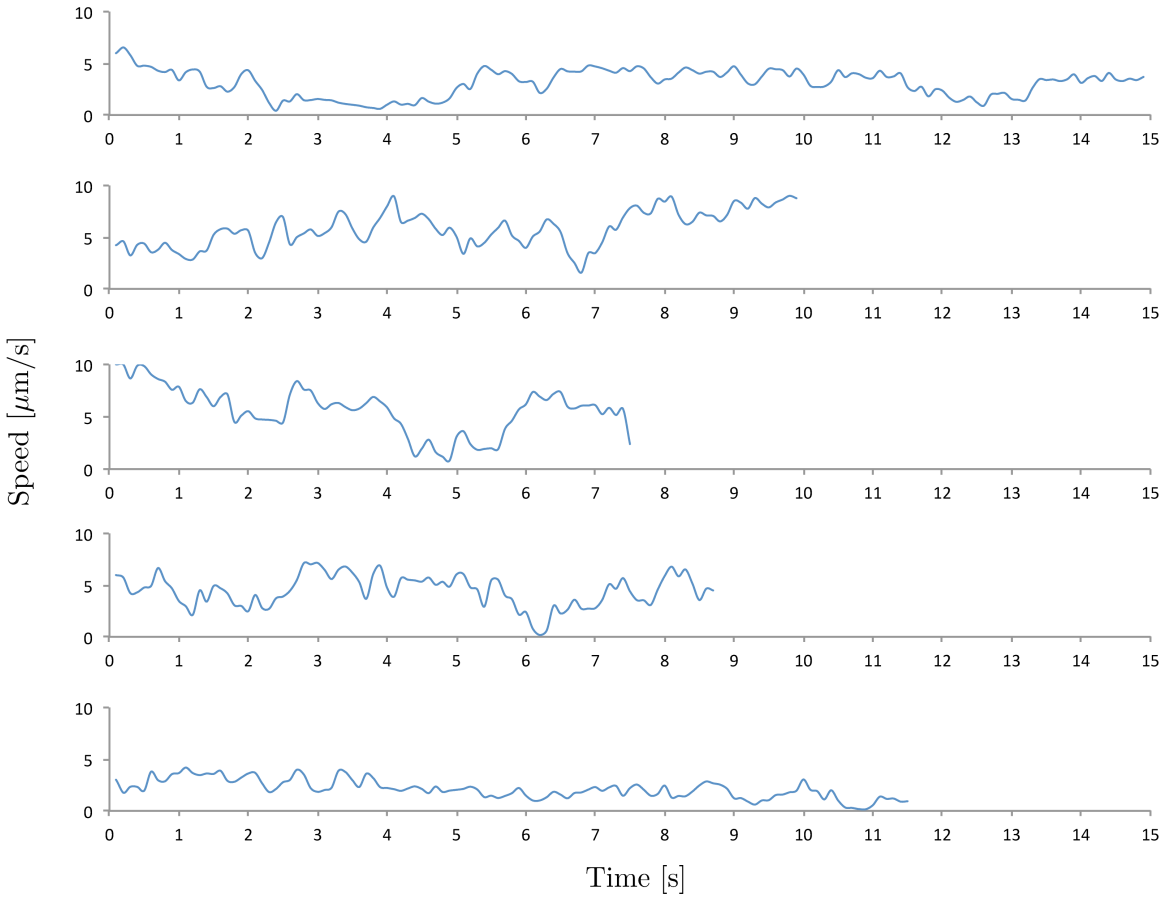

Figure S4. Five time series of *P. mirabilis* swimming speeds while pushing 2-μm diameter microparticles.

MATHEMATICAL MODEL

Numerical simulations

While the fluid anisotropy in the experiments clearly results in alignment and stability of the microorganism/cargo system, we studied a simpler model for the viscous flow, the isotropic Stokes equations, $\nabla p = \mu\nabla^2\boldsymbol{u}$ and $\nabla\cdot\boldsymbol{u} = 0$, where $\boldsymbol{u}$ is the fluid velocity, μ is the viscosity, and p is the pressure. The two equations represent conservation of momentum and mass, respectively. A fundamental (Green's function) solution to the Stokes equations is derived by inserting a point force $\boldsymbol{f}$ at a point $\boldsymbol{x}_0$ in an infinite fluid and solving $\nabla p = \mu\nabla^2\boldsymbol{u} + \boldsymbol{f}\delta(\boldsymbol{x}_0)$, where $\delta(\boldsymbol{x}_0)$ is a Dirac delta function (see [2]). The resulting velocity field is given by

$$\boldsymbol{u}(\boldsymbol{x}) = \boldsymbol{G}(\boldsymbol{x},\boldsymbol{x}_0)\cdot\boldsymbol{f}, \tag{1}$$

where

$$\boldsymbol{G}(\boldsymbol{x},\boldsymbol{x}_0) = \frac{1}{8\pi\mu}\left(\frac{\boldsymbol{I}}{r} + \frac{\boldsymbol{r}\boldsymbol{r}}{r^3}\right) \tag{2}$$

is known as the Stokeslet singularity. Here $\boldsymbol{I}$ the identity operator, $\boldsymbol{r} = \boldsymbol{x} - \boldsymbol{x}_0$, $r = |\boldsymbol{r}|$, and $\boldsymbol{r}\boldsymbol{r}$ is a dyadic product.

To compute the flow due to the motion of the cell body and spherical cargo driven by a line distribution of forcing, we employ the method of regularized Stokeslets by Cortez [3, 4]. A regularized Stokeslet is a smooth approximation to (2), constructed by solving the Stokes equations instead with a smoothed point force at $\boldsymbol{x}_0$, resulting in the solution $\boldsymbol{u}(\boldsymbol{x}) = \boldsymbol{G}_\delta(\boldsymbol{x},\boldsymbol{x}_0)\cdot\boldsymbol{f}$, where

$$\boldsymbol{G}_\delta(\boldsymbol{x},\boldsymbol{x}_0) = H_1(r)\boldsymbol{I} + H_2(r)\boldsymbol{r}\boldsymbol{r}, \tag{3}$$

$$H_1(r) = \frac{1}{8\pi\mu}\left(\frac{1}{(r^2+\delta^2)^{1/2}} + \frac{\delta^2}{(r^2+\delta^2)^{3/2}}\right), \quad H_2(r) = \frac{1}{8\pi\mu}\frac{1}{(r^2+\delta^2)^{3/2}}, \tag{4}$$

where δ is a small regularization parameter.

We compute the fluid flow on the microswimmer/cargo system by distributing regularized Stokeslet singularities on the surface of the cargo D_c, the surface of the cell body D_b, and along the length of the flagellum, D_f. The strengths $\boldsymbol{f}(\boldsymbol{x})$ of the singularities at each position are determined by the boundary conditions. Namely, the velocity is assumed to satisfy a no-slip condition on the cell body and cargo surfaces, so that $\boldsymbol{u} = \boldsymbol{U} + \boldsymbol{\Omega}\times\boldsymbol{x}$ there, with $\boldsymbol{U}$ the (as yet unknown) swimming speed and $\boldsymbol{\Omega}$ a rotation rate. On the flagellum, however, we specify the force distribution directly there with a strength f per unit length. With the symmetric system aligned with $\hat{\boldsymbol{x}}$, this results in a slip velocity $u_s(s)\hat{\boldsymbol{x}}$ along the flagellum (see [5]) where s is an arc-length parameter. To close the system we require there to be zero net force and zero net torque on the system. To summarize, we must invert the following system to determine the force distribution $\boldsymbol{f}$ on the load, the slip velocity u_s on the flagellum, the swimming speed $\boldsymbol{U}$ and the rotation rate $\boldsymbol{\Omega}$:

$$\boldsymbol{U} + \boldsymbol{\Omega}\times\boldsymbol{x} = \sum_{k=1}^{N}\boldsymbol{G}_\delta(\boldsymbol{x},\boldsymbol{y}_k)\cdot\boldsymbol{f}(\boldsymbol{y}_k) \quad \boldsymbol{x}\in D_b\cup D_c, \tag{5}$$

$$\boldsymbol{U} + \boldsymbol{\Omega}\times\boldsymbol{x} + u_s(s)\hat{\boldsymbol{x}} = \sum_{k=1}^{N}\boldsymbol{G}_\delta(\boldsymbol{x},\boldsymbol{y}_k)\cdot\boldsymbol{f}(\boldsymbol{y}_k) \quad \boldsymbol{x}\in D_f, \tag{6}$$

$$\boldsymbol{f}(\boldsymbol{x}) = -hf\hat{\boldsymbol{x}} \quad \boldsymbol{x}\in D_f, \tag{7}$$

$$\sum_{k=1}^{N}\boldsymbol{f} = \boldsymbol{0}, \quad \sum_{k=1}^{N}\boldsymbol{x}\times\boldsymbol{f} = \boldsymbol{0}. \tag{8}$$

The N points $\boldsymbol{y}_k$ are evenly distributed around the cell body, cargo, and flagellum so that the spacing between points, including the spacing between the cargo and the cell body, and the cell body and the flagellum, are equally spaced by a distance h. The system is solved by forming the linear matrix problem and inverting directly. Selecting the value of the regularization parameter is an artform; we use a form for δ used by Cortez et al. [4] which resulted in acceptable results in various test problems, $\delta = 0.22h^{0.9}$. By symmetry we expect $\boldsymbol{U} = U\hat{\boldsymbol{x}}$ and $\boldsymbol{\Omega} = \boldsymbol{0}$, which is confirmed in the computations. The value of N is chosen so that increasing N results in a departure from the presented results confined to within 5% of the reported values; generally this requires $N \approx 1000$.

In order to match the experiments we choose a cell body with aspect ratio $B/A = 0.4$, relative flagellum lengths L/A ranging

from 2 to 8, and relative cargo sizes A_c/A ranging from 0 to 2. The swimming speed of *P. mirabilis* in the experiments, absent cargo, is approximately $U = 9.6\ \mu$m/s, which we use to calibrate the force per unit length on the flagellum f. Using $L/A = 5$, we find approximately $f/\mu = 26.9\ \mu$m/s. The viscosity measured in the experiments, $\mu = 0.7$ Pa·s enters only to scale the force $\boldsymbol{f}$ and as such we neglect its inclusion; it's scale is implicit in the calibration process. The value f is the only fitting parameter used in the model.

Analytical estimate

We now describe three analytical estimates, each more accurate than the previous one. To obtain the simplest possible estimate of the swimming speed, we treat the total load (the cell body and cargo) as a single immersed sphere with an effective radius ρ, chosen so that the drag on the load moving with speed U (and with no flagellum) is given by $6\pi\mu\rho U$. For $A_c/A \gg 1$ we have $\rho \approx A_c$. For smaller values of A_c, we estimate the total drag on the load as the sum total of the drag on each component, neglecting hydrodynamic interactions, so that $\rho = A_c + K_e A$, where $e = \sqrt{1-(B/A)^2}$ is the eccentricity of the cell body, and

$$K_e = \frac{8e^3}{-6e + 3(1+e^2)\log[(1+e)/(1-e)]}. \tag{9}$$

This is the exact expression for the drag on a prolate spheroid (see [6]). With $B/A = 0.4$ we have $K_e \approx 0.522$. Neglecting hydrodynamic interactions with the flagellum, this expression may be used as the basis for an estimate of the swimming speed by simply insisting that the total force on the load is the total force generated by the flagellum, F, so that

$$U = \frac{F}{6\pi\mu\,(A_c + K_e A)}. \tag{10}$$

However, as shown in Fig. S5, where the computed values and estimate above are shown as solid and dashed lines, respectively, it is clear that this is a rather inaccurate estimate.

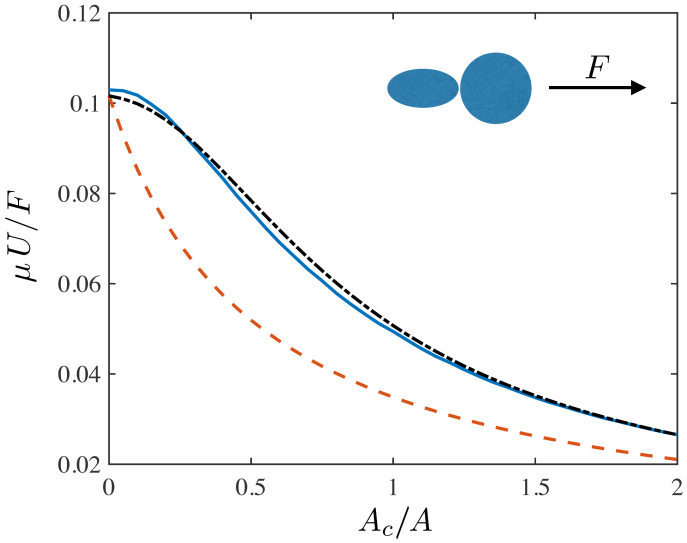

Figure S5. Two analytical estimate of the velocity of the load (assuming no hydrodynamic interactions between the cell body and the cargo) subject to a net force F, compared with the results of the full numerical simulations. Simulated values are shown as a solid line, the simplest estimate (10) is shown as a dashed line, and the improved estimate from (17) is shown as a dot-dashed line.

To obtain a more accurate approximation we include the leading order correction in a far-field expansion, now making the approximation that the cell body and cargo are well-separated. Writing the force on the cell-body as F_b and the force on the

cargo as F_c, we have

$$F_b = 6\pi\mu A K_e \left(U - u_c(\boldsymbol{x}_0)\right) + O\left(A^2\nabla^2 u_c\right), \tag{11}$$

$$F_c = 6\pi\mu A_c \left(U - u_b(\boldsymbol{x}_0 + (A + A_c)\hat{\boldsymbol{x}})\right) + O\left(A_c^2\nabla^2 u_b\right), \tag{12}$$

(see [6]) where $F_b + F_c = F$, and u_c and u_b are the velocity fields due to the motion of each component of the load separately (in an infinite fluid with no hydrodynamic interactions). The leading order flow field is given by the Stokeslet, i.e.

$$u_c(\boldsymbol{x}_0) = \hat{\boldsymbol{x}} \cdot \boldsymbol{G}(\boldsymbol{x}_0, \boldsymbol{x}_0 + (A + A_c)\hat{\boldsymbol{x}}) \cdot F_c\hat{\boldsymbol{x}}, \tag{13}$$

$$u_b(\boldsymbol{x}_0 + (A + A_c)\hat{\boldsymbol{x}}) = \hat{\boldsymbol{x}} \cdot \boldsymbol{G}(\boldsymbol{x}_0 + (A + A_c)\hat{\boldsymbol{x}}, \boldsymbol{x_0}) \cdot F_b\hat{\boldsymbol{x}}. \tag{14}$$

Combining the above, we find

$$F_b = \frac{AF(2A - A_c)K_e}{2A(A - 2A_c)K_e + 2A_c(A + A_c)}, \tag{15}$$

$$F_c = \frac{A_c F(2(A + A_c) - 3AK_e)}{2A(A - 2A_c)K_e + 2A_c(A + A_c)}, \tag{16}$$

$$U = \frac{F\left(4(A + A_c)^2 - 9AA_cK_e\right)}{24\pi\mu(A + A_c)(A(A - 2A_c)K_e + A_c(A + A_c))}, \tag{17}$$

matching the drag on a sphere of radius

$$\rho = \frac{4(A + A_c)(A(A - 2A_c)K_e + A_c(A + A_c))}{4(A + A_c)^2 - 9AA_cK_e}. \tag{18}$$

This estimated speed in (17) included as a dot-dashed line in Fig. S5, where it is seen to be a much more accurate approximation than (10).

While the estimate above is acceptable for the drag on the load, in the full swimming problem with flagellar forcing the prediction is inaccurate. As discussed in the main text, and shown in Fig. 4 there, it is important to include the hydrodynamic interaction of the flagellum with the load. Neglecting the flow due to the flagellum results in a considerable overestimate of the swimming speed. We therefore use the same approach as before but now we include the flow due to the nearly flagellum at leading order in a far-field calculation,

$$F_b = 6\pi\mu A K_e \left(U - u_c(\boldsymbol{x}_0) - u_f(\boldsymbol{x}_0)\right), \tag{19}$$

$$F_c = 6\pi\mu A_c \left(U - u_b(\boldsymbol{x}_0 + (A + A_c)\hat{\boldsymbol{x}} - u_f(\boldsymbol{x}_0 + (A + A_c)\hat{\boldsymbol{x}})\right), \tag{20}$$

where $F_b + F_c = F$ and u_f is a single Stokeslet of strength F placed at the center of the flagellum. This results in

$$\left(\frac{6\pi\mu A}{F}\right) U = \frac{C(\kappa, \lambda)}{D(\kappa, \lambda)}, \tag{21}$$

where

$$C(\kappa, \lambda) = 4(\kappa + 1)^2(\lambda + 2)(4 + \lambda - \kappa) + 3K_e\left\{\kappa\left(4\left(\kappa^2 + \kappa - 7\right) + 2(\kappa - 7)\lambda - 3\lambda^2\right) - 4(\lambda + 4)\right\}, \tag{22}$$

$$D(\kappa, \lambda) = 4(\kappa + 1)(\lambda + 2)(2\kappa + \lambda + 4)\left(\kappa^2 + \kappa - 2\kappa K_e + K_e\right), \tag{23}$$

with $\kappa = A_c/A$ and $\lambda = L/A$. Without cargo the swimming speed is given by (taking $\kappa \to 0$),

$$\left(\frac{6\pi\mu A K_e}{F}\right) U = 1 - \frac{3K_e}{2 + \lambda}. \tag{24}$$

[1] http://rsb.info.nih.gov/ij/plugins/track/track.html.

[2] C. Pozrikidis. *Boundary Integral and Singularity Methods for Linearized Viscous Flow*. Cambridge University Press, Cambridge, UK,

1992.
[3] R. Cortez. The method of regularized Stokeslets. *SIAM J. Sci. Comput.*, 23:1204–1225, 2001.
[4] J. Ainley, S. Durkin, R. Embid, P. Boindala, and R. Cortez. The method of images for regularized Stokeslets. *J. Comput. Phys.*, 227:4600–4616, 2008.
[5] D. Saintillan and M. J. Shelley. Orientational order and instabilities in suspensions of self-locomoting rods. *Phys. Rev. Lett.*, 99:058102, 2007.
[6] S. Kim and S. J. Karrila. *Microhydrodynamics: Principles and Selected Applications*. Dover Publications, Inc., Mineola, NY, 1991.